Phys. Lett. B 859 (2024) 139116

Contents lists available at ScienceDirect

Physics Letters B

journal homepage: www.elsevier.com/locate/physletb

Letter

New spin structure constraints on hyperfine splitting and proton Zemach radius

David Ruth [a,*], Karl Slifer [a], Jian-Ping Chen [b], Carl E. Carlson [c], Franziska Hagelstein [d,e,f], Vladimir Pascalutsa [d], Alexandre Deur [b], Sebastian Kuhn [g], Marco Ripani [h], Xiaochao Zheng [i], Ryan Zielinski [a], Chao Gu [j]

[a] University of New Hampshire, 03824, Durham, NH, USA
[b] Thomas Jefferson National Accelerator Facility, 23606, Newport News, VA, USA
[c] William & Mary, 23187, Williamsburg, VA, USA
[d] Institute of Nuclear Physics, Johannes Gutenberg Universität Mainz, 55099, Mainz, Germany
[e] PRISMA+ Cluster of Excellence, Johannes Gutenberg Universität Mainz, 55099, Mainz, Germany
[f] Laboratory for Particle Physics, Paul Scherrer Institute, 5232, Villigen PSI, Switzerland
[g] Old Dominion University, 23529, Norfolk, VA, USA
[h] Istituto Nazionale di Fisica Nucleare, Sezione di Genova, I-16146, Genova, Italy
[i] University of Virginia, 22903, Charlottesville, VA, USA
[j] Duke University, 27708, Durham, NC, USA

ARTICLE INFO

Editor: H. Gao

ABSTRACT

The 1S hyperfine splitting in hydrogen is measured to an impressive ppt precision and will soon be measured to ppm precision in muonic hydrogen. The latter measurement will rely on theoretical predictions, which are limited by knowledge of the proton polarizability effect Δ_{pol}. Data-driven evaluations of Δ_{pol} have long been in significant tension with baryon chiral perturbation theory. Here we present improved results for Δ_{pol} driven by new spin structure data, reducing the long-standing tension between theory and experiment and halving the dominating uncertainty in hyperfine splitting calculations.

1. Introduction

The hyperfine splitting in hydrogen, the renowned 21 cm line arising from the magnetic dipole interaction of electron and proton, stands out as one of the best-measured quantities in physics, currently known to an impressive 12 digits. This level of precision is challenging for theory to match, particularly in accounting for the effects of proton structure [1]. These structure effects are amplified in muonic hydrogen, where the hydrogen's electron is replaced by a muon. Presently, several high-profile experiments [2,3] are aiming at a first-ever measurement of the ground-state hyperfine splitting in muonic hydrogen. Their success in finding this forbiddingly narrow transition crucially depends on an accurate assessment of proton structure effects. However, previous determinations [4–6] of the leading uncertainty among these proton structure effects, the proton polarizability effect Δ_{pol}, have large error bars and are in significant tension with corresponding theoretical calculations [7], a crucial disagreement which can be seen in [8] and Fig. 3 of this paper. In this letter, we improve upon the evaluation of the proton polarizability contribution with new experimental proton spin structure data from the Thomas Jefferson National Accelerator Facility (JLab), significantly reducing this long-standing tension and halving this quantity's uncertainty.

The classical picture of the hydrogen atom is fairly simple: a pointlike spinless electron bound by a pointlike spinless proton via the Coulomb force. The Schrödinger equation gives the energy spectrum in natural units as $E_n = -\alpha^2 m_r/(2n^2)$, with n the principal quantum number and m_r the reduced mass. The more sophisticated picture of the atom is modeled as a correction to this simple picture, including the effects due to spin and the structure of the proton [9], to be discussed here. The proton structure effects are small, but clearly seen in the hydrogen spectrum at the current level of precision. They are more prominent in muonic hydrogen, because of a much smaller Bohr radius, $a_B = 1/(\alpha m_r)$, given that m_r goes roughly as the lepton mass, which is 200 times heavier for the muon. The muon has thus 200^3 greater probability [as given by the

* Corresponding author.
E-mail address: david.ruth@unh.edu (D. Ruth).

https://doi.org/10.1016/j.physletb.2024.139116
Received 6 August 2024; Received in revised form 8 October 2024; Accepted 3 November 2024
Available online 5 November 2024

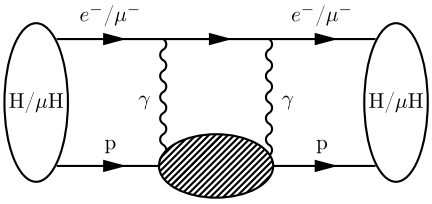

Fig. 1. Two-photon exchange diagram showing the interaction between electron (e^-) and proton (p) in hydrogen, or muon (μ^-) and proton in muonic hydrogen.

wave-function squared at the origin, $\left|\Psi_n(0)\right|^2 = 1/(\pi a_B^3 n^3)$] to be probing the proton substructure.

Because of this heightened sensitivity to nuclear structure details in muonic atoms, the recent breakthrough in the laser spectroscopy of muonic hydrogen (μH) by the CREMA Collaboration led to an order-of-magnitude improvement in the measurement of the proton charge radius [10,11]. Surprisingly to many, it appeared to be 7 σ smaller than the most-recent CODATA recommended value of the charge radius at the time [12]. This spectacular discrepancy, dubbed as the "proton radius puzzle" (see [13,14] for an early review) has seen significant progress towards its final resolution, and from 2018 onwards, CODATA recommends the smaller, and more precise, μH value. This chapter is not yet closed, with many new measurements of the proton charge radius underway using the conventional methods of normal hydrogen (H) spectroscopy, elastic electron-proton (ep) scattering and even muon-proton (μp) scattering, see [8,15,16] for recent reviews. Here we concern ourselves with the calculation of the μH hyperfine splitting (HFS), and its implications for the next milestone of μH spectroscopy: the upcoming experimental measurement of the μH ground-state HFS.

Two different collaborations are competing to provide this first-ever HFS measurement: CREMA [2] at the Paul Scherrer Institut (PSI) and FAMU [3] at the RIKEN-RAL Muon Facility. Given the extreme narrowness of this transition [17], their success depends in part on how well the proton-structure corrections are understood, since the searches can only be done over a very limited range of frequencies.

2. Proton structure in the HFS of hydrogen-like atoms

To leading order, $\mathcal{O}(\alpha^4)$, the HFS is given by the Fermi energy

$$E_{\rm F} = \frac{8\alpha}{3a_B^3}\frac{1+\kappa_p}{m_l M_p}, \tag{1}$$

where m_l is the lepton mass (either m_e in H or m_μ in μH), and M_p is the proton mass. Here the proton structure is only represented through the anomalous magnetic moment $\kappa_p = \frac{g_p - 2}{2}$.

At the next order, $\mathcal{O}(\alpha^5)$, the proton structure effects can all be computed via the two-photon (2γ) exchange diagram of Fig. 1, which usually is split into three contributions:

$$E^{2\gamma}_{nS\text{-HFS}} = \frac{E_{\rm F}}{n^3}\left(\Delta_Z + \Delta_{\rm recoil} + \Delta_{\rm pol}\right) \tag{2}$$

The largest, Δ_Z, comes from the proton Zemach radius R_Z [4,7,18–20], a measure of how far the electric and magnetic distributions of the proton are correlated with each other. R_Z is expressed in terms of the elastic electric and magnetic form factors $G_E(Q^2)$ and $G_M(Q^2)$:

$$R_Z = -\frac{4}{\pi}\int_0^\infty \frac{dQ}{Q^2}\left[\frac{G_E(Q^2)G_M(Q^2)}{g_p} - 1\right], \tag{3}$$

with g_p as the proton gyromagnetic g-factor. The recoil contribution $\Delta_{\rm recoil}$ can likewise be expressed in terms of the form factors [21], but the final contribution from the polarizability, $\Delta_{\rm pol}$, is more complicated.

The polarizability effect is caused by the proton's moments induced by the electromagnetic fields of the bound leptons. Unlike the radius, the polarizability contribution is not given by the form factors, but rather by the inelastic structure functions $g_{1,2}(x, Q^2)$, which are functions of the Bjorken x, a variable which tracks the fraction of the interaction's momentum carried by one of the proton's quark constituents as is defined kinematically as $x = \frac{Q^2}{2M\nu}$. This contribution is more difficult to obtain, due to the necessity to cover a 2-dimensional phase space, while the required spin structure function data are relatively sparse, especially at low Q^2 which dominates the determination. Previously, there had been only limited g_1 data and a complete lack of g_2 data in the kinematic region most relevant to the HFS. Nonetheless, a data-driven evaluation of this contribution has been attempted in the past [4–6].

The present status is that the existing data-driven evaluations, while consistent with each other, are in disagreement with chiral perturbation theory (χPT), which predicts a significantly smaller contribution of this effect [22,7].

Under the general assumptions of unitarity (optical theorem) and analyticity (dispersion relations) of the forward Compton scattering, the contribution of the spin structure functions has the following form [4,8]:

$$\Delta_{\rm pol} = \frac{\alpha m_l}{2\pi(1+\kappa_p)M_p}\left(\Delta_1 + \Delta_2\right), \tag{4}$$

$$\Delta_1 = \int_0^\infty \frac{dQ^2}{Q^2}\left[\beta_1(\tau_l)F_2^2(Q^2) + \frac{8M_p^2}{Q^2}\int_0^{x_{\rm th}} dx\,\tilde{\beta}_1(\tau,\tau_l)\,g_1(x,Q^2)\right], \tag{5}$$

$$\Delta_2 = -24M_p^2\int_0^\infty \frac{dQ^2}{Q^4}\int_0^{x_{\rm th}} dx\,\tilde{\beta}_2(\tau,\tau_l)\,g_2(x,Q^2) \tag{6}$$

where β's are elementary kinematic functions, τ's are kinematic variables, and F_2 is the Pauli form factor, the explicit definitions of which are in the Supplemental Materials. $x_{\rm th}$ corresponds to the minimum energy necessary to generate a pion, at an invariant mass W of 1073.2 MeV.

$\Delta_{\rm pol}$ currently dominates the theoretical uncertainty of HFS calculations [8,1] and it is evident that to calculate this contribution accurately, we must examine experimental measurements of the spin structure functions g_1 and g_2. Notably, the low-Q^2 regime dominates the integrals of Eqs. (5) and (6) due to the $\frac{1}{Q^2}$ and $\frac{1}{Q^4}$ factors, so it is especially vital to determine the spin structure functions at low Q^2 if we wish to fully understand the hydrogen atom, and by extension the HFS effect in general.

3. Data-driven evaluation of the polarizability effect

In the following, we focus on a new empirical input for the proton spin structure functions. Our evaluation entails new results from JLab Experiments E03-006 (EG4) and E08-027 (g2p), two complementary experiments both aimed at collecting low Q^2 data with longitudinally and transversely polarized proton (NH_3) targets, respectively [23,24]. Here, we present these experiments' contribution to the hyperfine integrals above, with the g2p data providing the first data-driven extraction of Δ_2, and the EG4 data providing new Δ_1 data with unprecedented coverage in the low-Q^2 region.

In the EG4 experiment, a longitudinally polarized electron beam with 1-3.5 nA of current was incident on a longitudinally polarized NH_3 target. The scattered electrons were detected using the CEBAF Large Acceptance Spectrometer (CLAS). The longitudinal polarized cross section difference $\Delta\sigma_\parallel$ was directly extracted from the yield difference between left- and right-handed beam electrons, such that contributions from the unpolarized material cancel. Combined with an estimation of the (small) transverse contribution based on a parameterization of world data, the proton structure function g_1 was extracted. Beam energies of 3.0, 2.3,

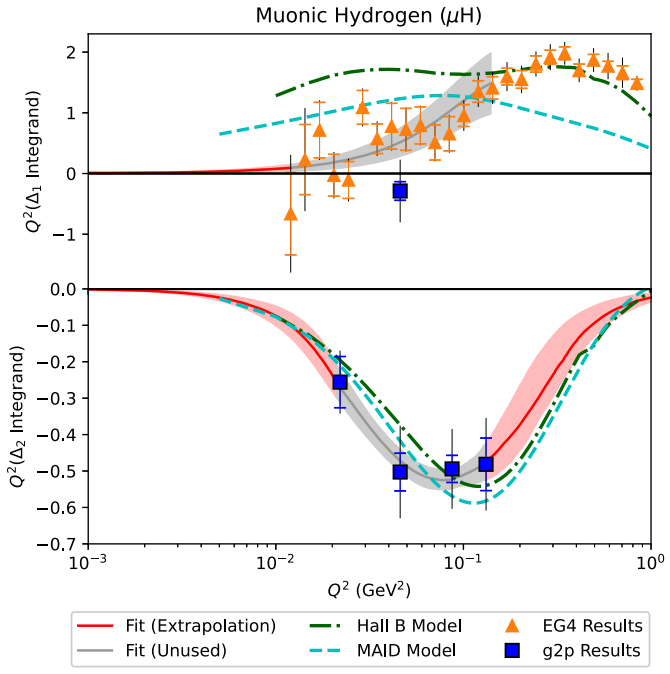

Fig. 2. The hyperfine contribution integrands for Δ_1 and Δ_2 in Eqs. (5) and (6), weighted by Q^2, for muonic hydrogen. Results from the g2p experiment [23] are shown in blue squares. The results of the EG4 experiment [24] are shown in orange triangles. The inner error bars represent the statistical uncertainty, while the outer error bars represent the total uncertainty including systematic error. The green dash-dot and cyan dashed lines represent the phenomenological Hall B and MAID models [25,26] respectively. The form factor term of the integrand for Δ_1 is constructed using the Arrington form factor fit [27]. The red line indicates a new phenomenological fit to the data and extrapolation to low $Q^2 = 0$ and high Q^2, with the red band representing the uncertainty of the calculation. The results are similar but have different mass scaling in electronic hydrogen.

2.0, 1.3, and 1.1 GeV were used, and along with the very small scattering angle down to 6°, enabled the experiment to reach a very low Q^2 of 0.012 GeV^2. These g_1 results were used to form the bulk of the low Q^2 Δ_1 data presented in this letter, see Fig. 2 (top panel).

In the g2p experiment, the parallel and perpendicular double spin asymmetries $A_\parallel$ and $A_\perp$ were measured for the scattering of polarized electrons with 50 nA current on longitudinally and transversely polarized NH_3 targets, respectively. Scattered electrons were detected at an angle of ≈6.5° using the Hall A High Resolution Spectrometers and a Septa Magnet. Measured asymmetries were combined with unpolarized cross section models from the Bosted-Christy phenomenological fit [28] to form polarized cross section differences, which were used to extract the spin structure functions. By varying the polarized target magnetic field's direction and the electron beam energy from 1.7 GeV to 3.3 GeV, five different kinematic settings were measured ranging from Q^2 of 0.02 GeV^2 to 0.12 GeV^2. Four of these settings were measured with a transverse polarized target field, giving rise to a perpendicular polarized cross section difference and a g_2 result, and one setting with a longitudinally polarized target field, which provides a parallel polarized cross section difference and a g_1 result. The results from the g2p experiment are the first data in a range relevant to the HFS, and so are used to form the Δ_2 results in this letter.

Results for the Δ_1 integrand are shown in the top of Fig. 2. The unmeasured part of the integral, largely at low Bjorken-x, is estimated using the CLAS Hall B model [25]. This is the best available model, containing significantly more modern g_1 data than the Simula parametrization [29] used in previous analyses [4]. A new phenomenological fit, shown in red, is generated to extrapolate to the low Q^2 region. Details on the fitting procedure can be found in the Supplemental Materials. Numerical results for these contributions are obtained by integrating over the data where they exist, primarily the EG4 data shown in [24], as well as data from the EG1b experiment in the Q^2 = 1.0-5.0 GeV^2 region [25]. The contribution from the low-Q^2 regime is calculated by integrating the displayed extrapolation fit, while the high-Q^2 contribution above Q^2 = 5.0 GeV^2 is calculated using the Hall B Model [25].

Results for the Δ_2 integrand in Eq. (6) are shown in the bottom of Fig. 2. The unmeasured part of the dx integral is again estimated using the Hall B model [25]. The results of g2p shown are the first ever direct experimental extractions of this quantity. The low and high Q^2 regions are calculated using the displayed fit, which is described in detail in the Supplemental Materials. Due to the comparative lack of g_2 data, the extrapolation has a somewhat larger error than for the Δ_1 results.

This historical lack of g_2 data makes it difficult to conclude if the Hall B model [25] is a good estimation of the low-x region or not. To account for this, we compare the result using the older Simula parametrization [29], which contains a significantly different prediction for the low-x behavior of g_2, and include the difference in our extrapolation error by comparing the upper and lower error bands of our extrapolating fit to the data in each case. Despite the very different models, this error contribution is relatively small, because the low-x region is suppressed for Δ_2.

The integrated results for Δ_1, Δ_2, and Δ_{pol} are as follows:

$$\Delta_1^e = 6.78 \pm 1.02(\text{data}) \pm 0.24(\text{extrapolation}) \tag{7}$$

$$\Delta_1^\mu = 5.69 \pm 0.84(\text{data}) \pm 0.20(\text{extrapolation}) \tag{8}$$

$$\Delta_2^e = -1.98 \pm 0.16(\text{data}) \pm 0.38(\text{extrapolation}) \tag{9}$$

$$\Delta_2^\mu = -1.40 \pm 0.11(\text{data}) \pm 0.31(\text{extrapolation}) \tag{10}$$

$$\Delta_{\text{pol}}^e = 1.09 \text{ ppm} \pm 0.31 \text{ ppm} \tag{11}$$

$$\Delta_{\text{pol}}^\mu = 200.6 \text{ ppm} \pm 52.4 \text{ ppm} \tag{12}$$

The total polarizability contribution to the hyperfine splitting is provided in parts per million (ppm) of the Fermi energy E_F. The uncertainties for Δ_1 and Δ_2 are divided into uncertainty coming directly from the data, and a combined systematic uncertainty coming from the extrapolations into high and low Q^2 regions and into the low-x regime. The extrapolation error is calculated by generating pseudo-data within the data's error bars, and calculating a new fit to this pseudo-data. This procedure is repeated 1000 times, and the standard deviation in the resulting fits is taken as the extrapolation error band (see the Supplemental Materials Appendix A). The total extrapolation error also includes a contribution from the choice of low-x fill-in model, where the highest upper band and lowest lower band achievable with different choices of fill-in model are taken as the absolute limits of the error band. The data error is a combination of statistical and systematic uncertainties from the respective experiments contributing to the result [23–25].

A reduced χ^2 (χ^2 per degree of freedom) test was performed on each fit for Δ_1 and Δ_2 to examine their performance. For this test the fit was compared to the set of data points used to create it, with number of points N_p and number of fit parameters N_f. The numerical results for reduced χ_ν^2 and degrees of freedom $\nu = N_p - N_f$ are as follows:

$$\Delta_1^H : \chi_\nu^2 = 1.831, \nu = 9 \tag{13}$$

$$\Delta_1^{\mu H} : \chi_\nu^2 = 2.253, \nu = 9 \tag{14}$$

$$\Delta_2^H : \chi_\nu^2 = 0.736, \nu = 1 \tag{15}$$

$$\Delta_1^{\mu H} : \chi_\nu^2 = 0.859, \nu = 1 \tag{16}$$

All of these values are within the 95% confidence interval based on degrees of freedom, with the exception of Δ_1 for μH, which is just barely outside that interval. The Δ_1 reduced χ_μ^2 is large because of the scatter in the EG4 data at low Q^2. By contrast, we seem to be slightly overfitting for Δ_2, this is difficult to avoid due to the relative lack of g_2 data. The muonic values are larger than the electronic values due to the smaller error bars resulting from the inclusion of the muon mass scaling.

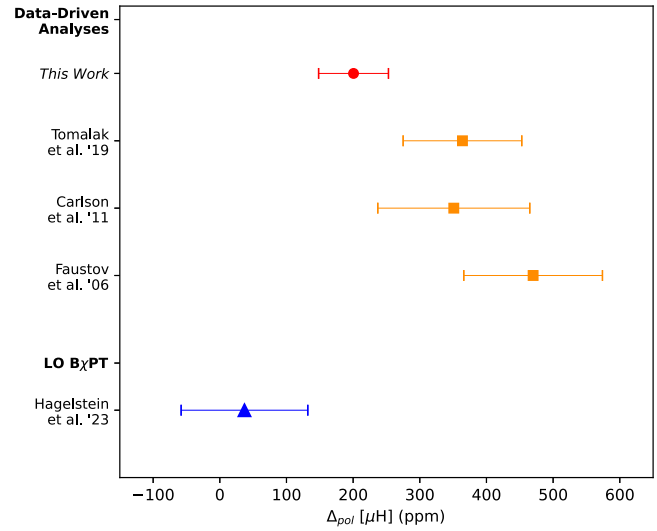

Fig. 3. The polarizability contribution to the hyperfine splitting for muonic hydrogen. One of the primary results of this analysis is shown in a red circle, and is compared to previous data-driven dispersion relation calculations [4–6] shown in orange squares, and the baryon chiral perturbation theory calculation [30,7,22] shown in blue triangles.

When considering the separate contributions from the two spin structure functions, Δ_1 and Δ_2, as shown above in equations (7) -(10), it is important to consider the contribution of the $\Delta(1232)$ resonance, the first excited state of the nucleon. Here, the $\Delta(1232)$ resonance will have large but opposite sign effects in Δ_1 and Δ_2 that cancel out in their sum almost completely. This effect, given by the one-loop 2γ-exchange diagram with the $\Delta(1232)$ intermediate state, has been estimated in [31] using large-N_c relations and empirical nucleon form factors.

As can be seen in Fig. 3, the new data from EG4 and g2p dramatically reduce the long standing discrepancy between the leading-order (LO) χPT prediction [30,7,22] and earlier data-driven dispersive evaluations [4–6] of the polarizability contribution. The large difference from the earlier dispersive results is illustrative of the importance of low-Q^2 data for Δ_{pol}, and the improvement in the available phenomenological models [25], which are constrained by a larger amount of data compared to earlier parametrizations used in previous analyses [29,32].

4. Implications for the proton Zemach radius

Our new data-driven evaluations of Δ_{pol} put us in the unique position to update the theoretical predictions of the HFS in (muonic) hydrogen, as well as the extractions of the proton Zemach radius from measurements of the HFS. The $1S$ HFS in H is extraordinarily well-measured [33,34]:

$$E^{\text{exp.}}_{1S\text{-HFS}}(\text{H}) = 1\,420.405\,751\,768(2)\,\text{MHz}. \tag{17}$$

Therefore, the presently most precise extraction of R_Z from spectroscopy is achieved when comparing the measured $1S$ HFS in H to the full theory prediction including QED, electroweak and strong interaction effects:

$$E_{nS\text{-HFS}} = \frac{E_{\text{F}}}{n^3}\left(1 + \Delta_{\text{QED}} + \Delta_{\text{weak}} + \Delta_{\text{strong}}\right). \tag{18}$$

For details on the numerical factors entering Eq. (18), we refer to the compilations in [8, Eq. (40) and (42)]. Here, Δ_{strong} contains the 2γ-exchange contributions introduced in Eq. (2), as well as other hadronic corrections such as hadronic vacuum polarization. The $\mathcal{O}(\alpha^5)$ recoil corrections Δ_{recoil} are taken from [35, Eq. (14) and (15)] and are consistent with our choice of F_2. Since the F_2 term in Δ_{pol} cancels exactly with a corresponding term in Δ_{recoil}, we do not need to take into account uncertainties of the F_2 parametrization in our Δ_{pol} evaluation. Note that

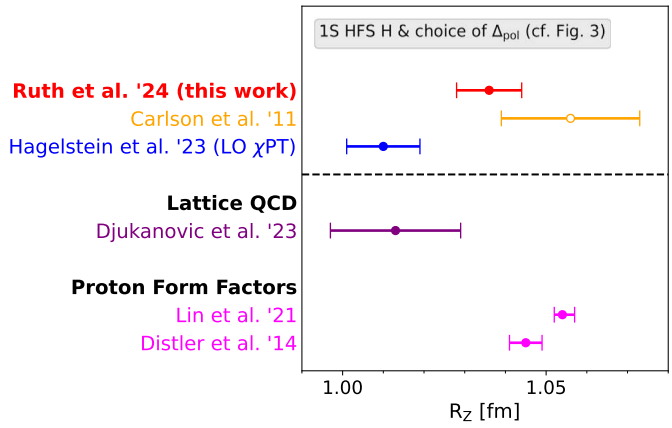

Fig. 4. Comparison of various extractions of the proton Zemach radius R_Z [4,7, 18–20].

radiative corrections (e.g., through electronic vacuum polarization) to the 2γ-exchange diagram are taken into account as well. The proton Zemach radius is then extracted from the $1S$ HFS in H as:

$$R_Z = 1.036(8)\,\text{fm}. \tag{19}$$

This result is more precise than previous extractions [1,36], as can be seen from the top panel of Fig. 4, where extractions of the Zemach radius from the measured $1S$ HFS in H are shown, assuming the same theoretical prediction of the HFS, but different values of Δ_{pol} as shown in Fig. 3. Our evaluation of Δ_{pol} based on new data for the proton spin structure functions (red), can be considered an update of the previous dispersive analysis [1] (orange open circle). It has moved closer to the extraction based on LO χPT (blue), but still does not agree. In the bottom panel of Fig. 4, recent precise results from lattice QCD suggest a small R_Z [18], in perfect agreement with the LO χPT extraction from the 1S H HFS, but in tension with evaluations based on proton form factors determined in scattering [19,20]. Our result is compatible with both [18] and [20].

Given the limited beam time and required tunability of the laser setup, precise theory guidance is crucial for the experiments planned by the CREMA [2] and FAMU [3] collaborations. Here we present an updated theory prediction for the $1S$ HFS in μH, based on the theory compilation in [8, Eq. (40)], and substituting our Δ_{pol}, as well as our extraction of the Zemach radius from the $1S$ HFS in H, cf. Eq. (19):

$$E^{\text{th.}}_{1S\text{-HFS}}(\mu\text{H}) = 182.636(16)\,\text{meV}. \tag{20}$$

This result, applying the H-rescaling as suggested in [37,38], is in perfect agreement with the presently most precise prediction presented in [8] of

$$E^{\text{th.}}_{1S\text{-HFS}}(\mu\text{H}) = 182.636(8)\,\text{meV}. \tag{21}$$

The latter result is based on a different rescaling of the precise empirical 1S HFS transition, cf. Eq. (17), utilizing the dependence of radiative corrections to the $\text{O}(\alpha^5)$ 2γ exchange on the type of hydrogen-like system (i.e., H or μH) and the principal quantum number n.

5. Conclusion

We present results for the first ever experimental data in a regime which contributes significantly to the integrals of the Δ_1 and Δ_2 Hyperfine Splitting contributions. This new data provides previously lacking guidance on how to constrain theoretical calculations of the Hyperfine Splitting effect. Previous data-driven work to determine these quantities [4] has been limited by older results lacking inelastic proton spin structure function data in the low Q^2 regime. These new results are much closer to agreement with χPT calculations of Δ_{pol}, strongly reducing the long-standing tension between different methods [8] and

reducing the overall error on the polarizability contribution by a factor of two. The reduction in uncertainty provided by the data of the EG4 and g2p collaborations is crucial in order to facilitate the search for the narrow μH $1S$ HFS in the planned experiments by the CREMA [2] and FAMU [3] Collaborations, as well as to interpret these future measurements. With these experiments aiming at up to 1 ppm relative precision, they have the potential to provide novel insights into the magnetic structure of the proton.

Declaration of competing interest

The authors declare the following financial interests/personal relationships which may be considered as potential competing interests: David Ruth reports financial support was provided by US Department of Energy under grant numbers DE-FG02-88ER40410 and DE-SC0024665. Karl Slifer, Ryan Zielinski report financial support was provided by US Department of Energy under grant DE-FG02-88ER40410. Xiaochao Zheng reports financial support was provided by US Department of Energy under grant DE-SC0014434. Carl E. Carlson reports financial support was provided by National Science Foundation grant PHY-181236. Franziska Hagelstein, Vladimir Pascalutsa report financial support was provided by Swiss National Science Foundation under grant PZ00P2_193383. Franziska Hagelstein, Vladimir Pascalutsa report financial support was provided by German Research Foundation through grant numbers 449369623 and 458854507. If there are other authors, they declare that they have no known competing financial interests or personal relationships that could have appeared to influence the work reported in this paper.

Acknowledgements

We thank Aldo Antognini and Vadim Lensky for their comments and discussions. This work was supported by the United States Department of Energy (DOE) under award numbers DE-FG02-88ER40410, DE-SC0024665, and DE-SC0014434, the National Science Foundation under grant PHY-181236, and by the Schweizerische Nationalfonds. This work is also supported by the Deutsche Forschungsgemeinschaft (DFG) through the Emmy Noether Programme Grant 449369623, the Research Unit FOR5327 Grant 458854507, and by the Swiss National Science Foundation (SNSF) through the Ambizione Grant PZ00P2_193383. This material is based upon work supported by the U.S. Department of Energy Office of Science, Office of Nuclear Physics under contract DE-AC05-06OR23177.

Appendix A. Supplemental materials

In this section, we describe our evaluation of Δ_1 and Δ_2 in detail. The formalism presented in the main text agrees with [4]. Since the elastic form factor contribution and the structure function contribution to the Δ_1 integral at low Q^2 are both large, but enter with opposite sign, their combination is very sensitive to systematic error. Therefore, it is advantageous to use the notation from [8] that explicitly splits Δ_1 into a contribution from $I_1^{\rm pol}$ and a fast convergent remainder:

$$\Delta_1 = 4\int_0^\infty \frac{dQ^2}{Q^2}\left[\beta_1(\tau_l) I_1^{\rm pol}(Q^2) + \frac{2M_p^2}{Q^2}\int_0^{x_{\rm th}} dx\,\tilde{\beta}_1(\tau,\tau_l)\,g_1(x,Q^2)\right], \tag{A.1}$$

$$\Delta_2 = -24 M_p^2 \int_0^\infty \frac{dQ^2}{Q^4}\int_0^{x_{\rm th}} dx\,\tilde{\beta}_2(\tau,\tau_l)\,g_2(x,Q^2) \tag{A.2}$$

with the polarizability part of the generalized GDH(Gerasimov-Drell-Hearn) integral $I_1(Q^2)$:

$$I_1^{\rm pol}(Q^2) = \frac{F_2^2(Q^2)}{4} + I_1(Q^2) \tag{A.3}$$

$$= \frac{F_2^2(Q^2)}{4} + \frac{2M_p^2}{Q^2}\int_0^{x_{\rm th}} dx\,g_1(x,Q^2) \tag{A.4}$$

This choice allows us to more easily resolve the extrapolation to $Q^2 = 0$, where form factor and structure function contribution cancel exactly due to the GDH sum rule [39–41], yielding $I_1^{\rm pol}(0) = 0$. In the above, and in the main text eqs. (5) and (6), the following auxiliary functions are employed:

$$\tilde{\beta}_1(\tau,\tau_l) = \frac{x^2\beta_1(\tau) - (\frac{m_l}{M_p})^2\beta_1(\tau_l)}{x^2 - (\frac{m_l}{M_p})^2}, \tag{A.5}$$

$$\tilde{\beta}_1(\tau,\tau_l) = \frac{x^2[\beta_1(\tau) - \beta_1(\tau_l)]}{x^2 - (\frac{m_l}{M_p})^2}, \tag{A.6}$$

$$\beta_1(\tau) = -3\tau + 2\tau^2 + 2(2-\tau)\sqrt{\tau(\tau+1)}, \tag{A.7}$$

$$\tilde{\beta}_2(\tau,\tau_l) = \frac{x^2[\beta_2(\tau) - \beta_2(\tau_l)]}{x^2 - (\frac{m_l}{M_p})^2}, \tag{A.8}$$

$$\beta_2(\tau) = 1 + 2\tau - 2\sqrt{\tau(\tau+1)}. \tag{A.9}$$

M_p and m_l represent the masses of the proton and lepton respectively, where the lepton is an electron for normal hydrogen or a muon for muonic hydrogen. Eqs. (A.5)-(A.9) contain the dimensionless quantities: $\tau = \frac{\nu^2}{Q^2} = \frac{Q^2}{4M_p^2x^2}$, $\tau_p = \frac{Q^2}{4M_p^2}$, and $\tau_l = \frac{Q^2}{4m_l^2}$.

F_2 is the Pauli form factor, which can be written in terms of the Sachs electromagnetic form factors as:

$$F_2(Q^2) = \frac{G_M(Q^2) - G_E(Q^2)}{1+\tau_p}, \tag{A.10}$$

We employ the Arrington et al. form factor parametrization [27] to obtain the values of G_E and G_M, and by extension, of F_2. We have checked that our results change by less than 1% when using the dispersive form factor description from [19].

The data of EG4 [24] and g2p [23] are integrated across Bjorken-x using a Simpson's rule integration to form the dx integral of (A.1) and (A.2). These data have already been adjusted to constant Q^2 in their respective independent analyses, so for each set of constant Q^2 data, we can perform one dx integration and get one point of the overall dQ^2 integration. The data starts very close to the pion production threshold and ends around an invariant mass of W = 2500 MeV, depending on the experiment and kinematic setting, so there is an unmeasured high W (or low x) region which we fill in with the CLAS Hall B model [25]. This has a small effect on Δ_2 and a more significant effect on Δ_1. We use the difference between this model and the older Simula parametrization [29] as a systematic uncertainty, discussed further at the end of this section.

Since the data does not extend fully to $Q^2 = 0$ or ∞, it is necessary to extrapolate into the regions with no data, as mentioned in the text. For Δ_1, we perform a simple second order polynomial fit to the fastly convergent term containing $\overline{\beta}_1$(Second line in (A.1)):

$$\Delta_1^{\rm Fast}({\rm Fit}) = A_1Q^6 + B_1Q^4 + C_1Q^2. \tag{A.11}$$

We can also obtain an excellent fit to $I_1^{\rm pol}$ with the functional form:

$$I_1^{\rm pol}({\rm Fit}) = \frac{Q^2}{A_2^2}\left(1 + \frac{Q^2}{B_2^2}\right)^{-3}, \tag{A.12}$$

with A, B as free parameters. These fits are added together with the appropriate kinematic weighting to obtain the total Δ_1 integrand fit shown in the main text.

Table A.1
Fit parameters for the central value of each of the above fits.

	A	B	C
H Polynomial($_1$)	215.95 ± 8.69	-112.06 ± 3.96	14.61 ± 0.44
μH Polynomial ($_1$)	410.30 ± 17.45	-213.03 ± 7.85	27.84 ± 0.85
H I_1^{pol}($_2$)	0.42 ± 0.39	-0.99 ± 0.71	
μH I_1^{pol}($_2$)	0.41 ± 0.39	-0.94 ± 0.53	
H Pade($_3$)	-4.20e-4 ± 2.41e-4	-1.19 ± 0.61	-38.630 ± 23.56
μH Pade($_3$)	-1.04e-3 ± 0.19e-3	-1.55 ± 0.99	-30.068 ± 13.98

Table A.2
Systematic contributions to Δ_1 and Δ_2. The errors listed are combined with statistical error on the data from [23,24] to obtain the values given in the main text.

	Source	H	μH
Δ_1 Data	Data Systematics	0.09	0.06
Δ_1 Extrap.	High-W Model	0.03	0.02
	Low Q^2 Fit	0.20	0.18
Δ_2 Data	Data Systematics	0.08	0.06
Δ_2 Extrap.	High-W Model	0.10	0.09
	Low Q^2 Fit	0.17	0.12
	High Q^2 Fit	0.11	0.10

The Δ_2 high Q^2 fit extrapolation is performed with a Pade fit:

$$\Delta_2(\text{Fit}) = \frac{Q^4}{A_3 + B_3 Q^4 + C_3 Q^8}. \tag{A.13}$$

These functional forms produce very good fits to the data, but the choice of fit for both quantities is somewhat arbitrary, if guided partially by knowledge of the low-Q^2 behavior. We quantify this arbitrary choice by comparing several fit functional forms, and including the difference between them as a systematic in our listed extrapolation error. For Δ_1, the careful balancing of the F_2 and I_1 terms makes this more difficult, because a pathologic fit could have a large impact on the total integral, leading to a larger resulting systematic. The fit parameters we find for the central value of each fit are provided in Table A.1.

Since the weighting of the Δ_1 and Δ_2 integrands depends on τ_l, and thus the ratio of Q compared to the lepton mass m_l, the H case receives larger contributions from the low-Q region. As a consequence, there is a stronger impact of the extrapolation uncertainties on the H case, as can be seen from Table A.2. It is therefore important to have a meaningful functional form for the extrapolation into the unmeasured low-Q region. Ref. [4] found a numerical approximation for the kernel function $\beta_1(\tau, \tau_l)$ at low Q. Analogously, we find a numerical approximation for the kernel function in the Δ_2 integral:

$$\tilde{\beta}_2(\tau, \tau_l) \approx \beta_2(\tau_l)\, \frac{\tau_l}{\tau} \left(1 - \frac{1}{4\tau}\right). \tag{A.14}$$

The above approximation was derived as an educated guess. The Q^2-integrand of Δ_2 is then proportional to $\beta_2(\tau_l)\tau_l$ and was fixed to the lowest data point from the g2p experiment. Note that this is similar to describing the low-Q region from $Q^2 = 0$ to Q_0^2 through an expansion in lowest-order spin polarizabilities:

$$\Delta_2[0, Q_0^2] = \frac{6M_p^2}{\alpha} \left[\gamma_0 - \delta_{LT}\right] \int_0^{Q_0^2} dQ^2 \beta_2(\tau_l)\, \tau_l, \tag{A.15}$$

where γ_0 and δ_{LT} are the forward spin and longitudinal transverse polarizabilities, respectively.

The breakdown of systematic contributions is shown in Table A.2. The remaining error from the results of the main text comes from the statistical error of the data. Information on the systematics of the data can be found in the publications focused on each dataset [23,24]. The low-x model systematics are estimated by comparing the impact of the Simula [32] and Hall B [25] models. For Δ_1, we disregard the difference between the two models at very low Q^2, as the difference becomes drastic and the Hall B model includes substantially more relevant and recent data in its fit. The strange behavior of the Simula parametrization in this region seems to reflect its relative lack of lower Q^2 data rather than a true uncertainty in our result. Both models agree very reasonably well at intermediate and higher Q^2. For both Δ_1 and Δ_2, the low-x contribution would contribute more alone, but it is convoluted together with the uncertainty of the low-Q^2 fit: the Q^2 fit was repeated with each model and the total upper and lower error band was used to obtain the uncertainty. The numbers given in this table are reflective of how much more the low-x uncertainty adds to the total result on top of what would be obtained from the low-Q^2 fit alone. The fit uncertainty for high and low-Q^2 is obtained by randomly scattering the data within its error bars and performing a fit, then iterating this process 1000 times and taking the average fit and standard deviation as the central fit and error band, respectively. This error is then increased by repeating this process with several viable functional forms and taking the maximal and minimal error band achieved as the total limit of the fit uncertainty. This is the number quoted in the above table. It is plain to see that the dominating systematic is related to the low-Q^2 fit for Δ_1, and both the high and low Q^2 fits for Δ_2. This may be further improved if future experiments are able to collect high precision measurements of the spin structure functions g_1 and g_2 at even lower Q^2, and of g_2 in the transition region of intermediate Q^2.

Data availability

Data will be made available on request.

References

[1] A.V. Volotka, V.M. Shabaev, G. Plunien, G. Soff, Eur. Phys. J., D, At. Mol. Opt. Phys. (ISSN 1434-6079) 33 (2005) 23.
[2] P. Amaro, et al., SciPost Phys. 13 (2022) 020, arXiv:2112.00138 [physics.atom-ph].
[3] C. Pizzolotto, et al., Eur. Phys. J. A 56 (2020) 185.
[4] C.E. Carlson, V. Nazaryan, K. Griffioen, Phys. Rev. A 78 (2008) 022517.
[5] Oleksandr Tomalak, Eur. Phys. J. A 55 (2019) 64.
[6] R. Faustov, I. Gorbacheva, A. Martynenko, Spie Digital Library, Bellingham, WA, https://doi.org/10.1117/12.696903, 2006.
[7] F. Hagelstein, V. Lensky, V. Pascalutsa, Eur. Phys. J. C (ISSN 1434-6052) 83 (2023) 762.
[8] A. Antognini, F. Hagelstein, V. Pascalutsa, Annu. Rev. Nucl. Part. Sci. 72 (2022) 389.
[9] K. Pachucki, V. Lensky, F. Hagelstein, S.S. Li Muli, S. Bacca, R. Pohl, Rev. Mod. Phys. 96 (2024) 015001, arXiv:2212.13782 [physics.atom-ph].
[10] R. Pohl, et al., Nature 466 (2010) 213.
[11] A. Antognini, F. Nez, K. Schuhmann, F.D. Amaro, F. Biraben, J.M.R. Cardoso, D.S. Covita, A. Dax, S. Dhawan, M. Diepold, L.M.P. Fernandes, A. Giesen, A.L. Gouvea, T. Graf, T.W. Hänsch, P. Indelicato, L. Julien, C.-Y. Kao, P. Knowles, F. Kottmann, E.-O.L. Bigot, Y.-W. Liu, J.A.M. Lopes, L. Ludhova, C.M.B. Monteiro, F. Mulhauser, T. Nebel, P. Rabinowitz, J.M.F. dos Santos, L.A. Schaller, C. Schwob, D. Taqqu, J.F.C.A. Veloso, J. Vogelsang, R. Pohl, Science 339 (2013) 417, https://www.science.org/doi/pdf/10.1126/science.1230016.
[12] P.J. Mohr, B.N. Taylor, D.B. Newell, Rev. Mod. Phys. 84 (2012) 1527.
[13] C.E. Carlson, Prog. Part. Nucl. Phys. 82 (2015) 59, arXiv:1502.05314 [hep-ph].
[14] R. Pohl, R. Gilman, G.A. Miller, K. Pachucki, Annu. Rev. Nucl. Part. Sci. 63 (2013) 175, arXiv:1301.0905 [physics.atom-ph].
[15] J.-P. Karr, D. Marchand, E. Voutier, Nat. Rev. Phys. 2 (2020) 601.
[16] H. Gao, M. Vanderhaeghen, Rev. Mod. Phys. 94 (2022) 015002, arXiv:2105.00571 [hep-ph].
[17] J. Nuber, et al., SciPost Phys. Core 6 (2023) 057, arXiv:2211.08297 [physics.atom-ph].
[18] D. Djukanovic, G. von Hippel, H.B. Meyer, K. Ottnad, M. Salg, H. Wittig, arXiv:2309.17232 [hep-lat], 2023.
[19] Y.-H. Lin, H.-W. Hammer, U.-G. Meißner, Phys. Rev. Lett. 128 (2022) 052002, arXiv:2109.12961 [hep-ph].
[20] M.O. Distler, J.C. Bernauer, T. Walcher, Phys. Lett. B 696 (2011) 343, arXiv:1011.1861 [nucl-th].
[21] C.E. Carlson, V. Nazaryan, K. Griffioen, Phys. Rev. A 83 (2011) 042509, arXiv:1101.3239 [physics.atom-ph].
[22] F. Hagelstein, V. Pascalutsa, PoS CD15 (2016) 077.

[23] D. Ruth, R. Zielinski, C. Gu, et al., Nat. Phys. 18 (2022) 1441.
[24] X. Zheng, A. Deur, H. Kang, et al., Nat. Phys. 17 (2021) 736.
[25] R. Fersch, et al., CLAS Collaboration, Phys. Rev. C 96 (2017) 065208.
[26] D. Drechsel, S.S. Kamalov, L. Tiator, Eur. Phys. J. A (ISSN 1434-601X) 34 (2007) 69.
[27] J. Arrington, Phys. Rev. C 69 (2004) 022201.
[28] M.E. Christy, P.E. Bosted, Phys. Rev. C 81 (2010) 055213.
[29] S. Simula, M. Osipenko, G. Ricco, M. Taiuti, Phys. Rev. D 65 (2002) 034017.
[30] F. Hagelstein, V. Lensky, V. Pascalutsa, Eur. Phys. J. C 83 (2023) 762, arXiv:2305.09633 [nucl-th].
[31] F. Hagelstein, Few Body Syst. 59, https://doi.org/10.1007/s00601-018-1403-x, arXiv:1801.09790 [nucl-th].
[32] S. Simula, et al., in: Proceedings, 2nd International Symposium GDH 2002, Genova, Italy, July 3-6, 2002, INSPIRE, 2002, arXiv:nucl-th/0212031 [nucl-th].
[33] H. Hellwig, R.F.C. Vessot, M.W. Levine, P.W. Zitzewitz, D.W. Allan, D.J. Glaze, IEEE Trans. Instrum. Meas. (ISSN 0018-9456) 19 (1970) 200.
[34] S.G. Karshenboim, Can. J. Phys. 78 (2000) 639, arXiv:physics/0008051.
[35] A. Antognini, Y.-H. Lin, U.-G. Meißner, Phys. Lett. B 835 (2022) 137575, arXiv:2208.04025 [nucl-th].
[36] A. Antognini, F. Kottmann, F. Biraben, P. Indelicato, F. Nez, R. Pohl, Ann. Phys. 331 (2013) 127, arXiv:1208.2637 [physics.atom-ph].
[37] O. Tomalak, Eur. Phys. J. A 54 (2018) 3, arXiv:1709.06544 [hep-ph].
[38] C. Peset, A. Pineda, J. High Energy Phys. 04 (2017) 060, arXiv:1612.05206 [nucl-th].
[39] S.B. Gerasimov, Yad. Fiz. 2 (1965) 598.
[40] S.D. Drell, A.C. Hearn, Phys. Rev. Lett. 16 (1966) 908.
[41] M. Hosoda, K. Yamamoto, Prog. Theor. Phys. 36 (1966) 425.